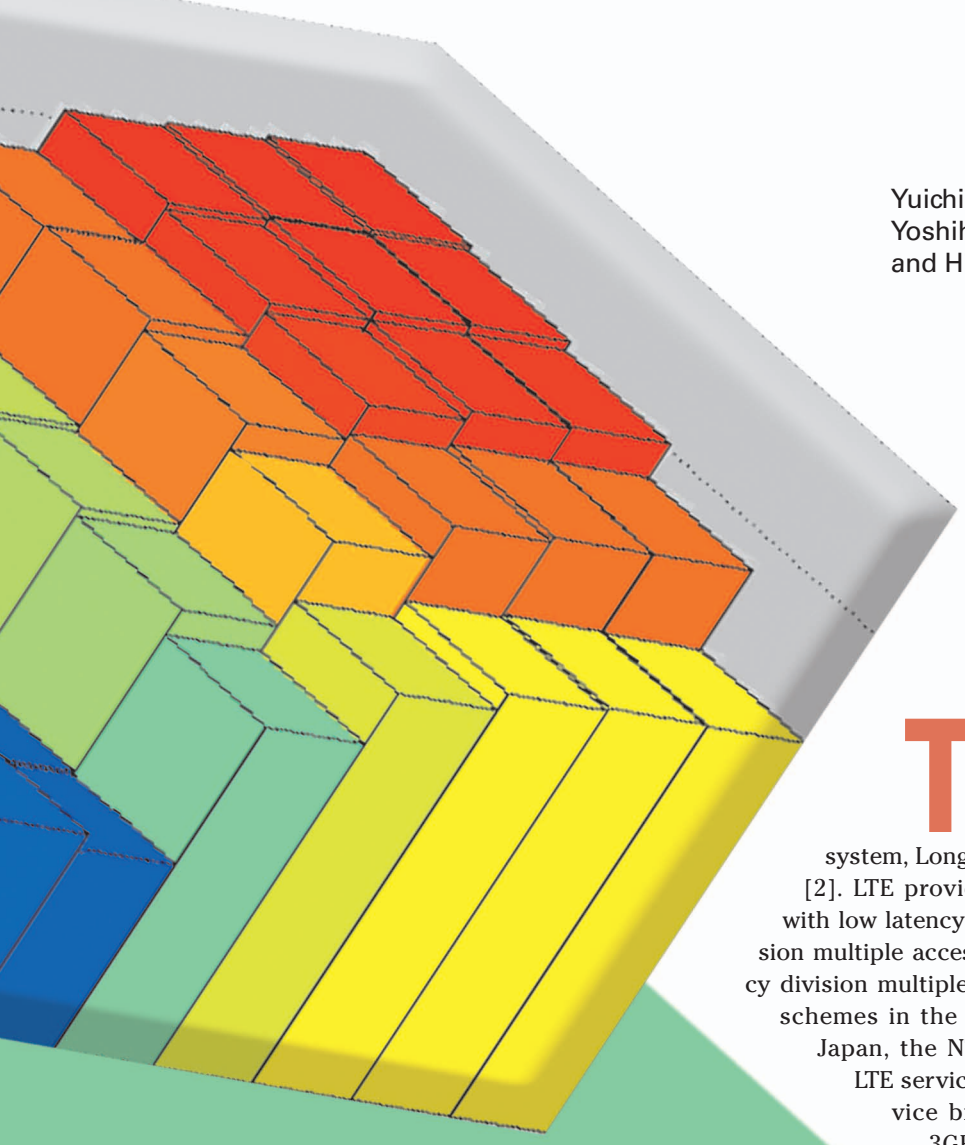


Yuichi Kakishima, Teruo Kawamura, Yoshihisa Kishiyama, Hidekazu Taoka, and Hidehiro Andoh

Evaluating Downlink MU-MIMO

Laboratory Experimentation and Results

The Third Generation Partnership Project (3GPP) finalized the radio interface specifications for the next generation mobile communication system, Long Term Evolution (LTE), as Release 8 [1], [2]. LTE provides full IP packet-based radio access with low latency and adopts orthogonal frequency division multiple access (OFDMA) and single-carrier frequency division multiple access (SC-FDMA) as multiple access schemes in the downlink and uplink, respectively. In Japan, the NTT DOCOMO launched a commercial LTE service in December 2010 under the new service brand "Xi" (crossy) [3]. Meanwhile, in 3GPP standardization, there have been efforts toward establishing an enhanced LTE radio interface, LTE-Advanced (LTE Release 10 and beyond), and specifications for LTE Release 10 were finalized [4], [5]. In LTE-Advanced, it is necessary to support a wider bandwidth than that in LTE Release 8, i.e., 20 MHz, to satisfy the high level requirements corresponding to the target peak data rate of greater than 1 Gb/s. To this end, LTE-Advanced supports carrier aggregation (CA) up to 100 MHz by aggregating multiple component carriers (CCs) with backward compatibility to LTE Release 8. In addition, to satisfy the requirements for further improvement in terms of spectrum efficiency, enhanced multiple-input multiple-output (MIMO) techniques such as higher-order MIMO multiplexing and multi-user (MU)-MIMO are supported.

Digital Object Identifier 10.1109/MVT.2012.2218435
Date of publication: 10 December 2012

Enhanced MU-MIMO in the downlink is an essential technique to satisfy the International Mobile Telecommunication (IMT)-Advanced requirements for cell spectrum efficiency and cell-edge spectrum efficiency in macro-cellular and base coverage urban environments [14]. In LTE-Advanced, two types of reference signals (RSs) are newly defined: the RS used for channel state information (CSI) estimation, i.e., CSI-RS, and the RS used for data demodulation (DM), i.e., DM-RS. These RSs enable enhanced MU-MIMO with inter-user interference control in the LTE-Advanced. The higher-rank transmission using MU-MIMO is beneficial because using single-user (SU)-MIMO is often limited by the number of antennas for a set of user equipment (UE). When the base station (BS) spatially multiplexes the maximum of four data streams, which exceeds the number of receiver antennas per mobile station (MS), very accurate CSI feedback is required so that the BS can generate precoding weights to reduce the mutual interference between the transmitted data streams of spatially multiplexed MSs [6]–[8]. Therefore, in our experimental equipment, we implement extended CSI feedback based on eigenvalue decomposition (EVD) to evaluate the potential performance of LTE-Advanced MU-MIMO, although it is not yet standardized as an LTE-Advanced specification.

In [6], we reported that, in laboratory experiments using a multipath fading simulator, the total downlink throughput performance of 1 Gb/s is achieved by applying four-by-two MU-MIMO to two MSs using CA with five CCs (90-MHz bandwidth) based on experimental equipment employing the LTE-Advanced radio interface such as DM-RS and CSI-RS. In this article, we further evaluate the influence of the number of CSI feedback quantization bits for the eigenvectors per subband (SB) on the achievable throughput performance for four-by-two MU-MIMO applying adaptive modulation and coding (AMC) and hybrid automatic repeat request (HARQ) in the laboratory experiments. In the study, we assume two LTE-Advanced deployment scenarios: i.e., cellular environments employing high-elevation BS antennas with high correlated fading channel and indoor/small cell environments employing BS antennas with uncorrelated fading channel. In addition to MU-MIMO, we evaluate the throughput performance for four-by-two SU-MIMO, where the precoding is generated based on CSI feedback that is identical to that for MU-MIMO. We also clarify the throughput performance for MU-MIMO considering the number of CSI feedback quantization bits in an indoor office environment.

We also clarify the throughput performance for MU-MIMO considering the number of CSI feedback quantization bits in a real indoor propagation environment.

MU-MIMO Scheme for Experimental Evaluations

Time/Frequency Granularity for MU-MIMO Operation

In this article, downlink MU-MIMO with a single BS and two MSs is evaluated in laboratory and indoor experiments, where the number of BS transmitter antennas, N_{TX}, is four, the number of receiver antennas for each MS, N_{RX}, is two, and the maximum number of data streams per MS is two. Figure 1 presents the RS structure for the implemented LTE-Advanced transceiver for Rank-4 MU-MIMO. In the frequency domain, each CC consists of multiple SBs, where N_S is the number of SBs per CC. Each SB has the bandwidth of F_{CSI} and consists of multiple resource blocks (RBs), each of which contains 12 subcarriers (= 180 kHz). An SB is a unit of CSI feedback. In the time domain, the subframe duration, that is, transmission time interval (TTI), is 1 ms, which contains 14 OFDMA symbols. The RS used for CSI estimation, that is, CSI-RS, for each transmitter antenna is periodically multiplexed with the time duration of several TTIs, T_{CSI}, where the CSI-RS for each transmitter antenna is multiplexed using frequency division multiplexing and mapped every six subcarriers. Thus, the precoding weights for MU-MIMO operation are updated with the same periodicity as that for the CSI-RS with the additional control delay of 10 ms. The RS used to demodulate each data stream, that is, the DM-RS, which is precoded in the same manner as the data streams, is multiplexed with the insertion density of 12 resource elements (REs) per RB per stream and within each subframe. For Rank-4 MU-MIMO, code division multiplexing is used to multiplex

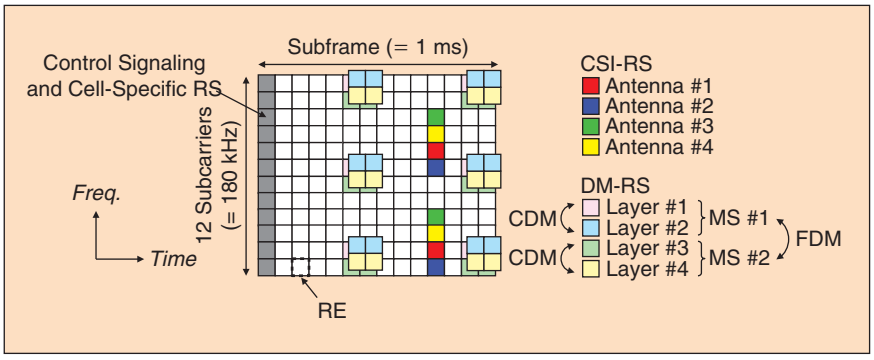


Figure 1 RS structure for implemented LTE-Advanced transceiver (Rank-4 MU-MIMO).

For Rank-4 MU-MIMO, code division multiplexing is used to multiplex DM-RSs between two data streams within the same MS, and FDM is used between two MSs. For Rank-2 MU-MIMO, CDM is applied to multiplex the DM-RSs between two MSs.

DM-RSs between two data streams within the same MS, and FDM is used between two MSs. For Rank-2 MU-MIMO, CDM is applied to multiplex the DM-RSs between two MSs.

CSI Feedback Scheme and Quantization

The MS calculates the CSI as feedback information and notifies the BS. The MS calculates the eigenvectors and the eigenvalues of the covariance matrix of the measured channel, and the received signal-to-interference plus noise power ratio (SINR) for each SB. At the u-th MS (u = 1 or 2), the downlink channel matrix ($N_{RX} \times N_{TX}$) on the k-th subcarrier, $\mathbf{H}_u(k)$, is estimated using the received CSI-RS, which is denoted as $\hat{\boldsymbol{H}}_u(k)$. Then, the covariance matrix for each SB, $\bar{R}_u$, is calculated by averaging $\hat{H}_u^H(k)\hat{H}_u(k)/S_u$ within the SB in the frequency and time domains, where S_u is the average received CSI-RS power for the normalization to remove the effect of path loss and shadowing. Below, the calculation of the CSI feedback, which is calculated for each SB is presented and the index of the SB is omitted for simplicity. By applying the Jacobi EVD [10] to the channel covariance matrix as $\bar{R}_u = U_u D_u^2 U_u^H$, eigenvalues $D_u^2 = diag\{\lambda_{u,1}^2, \lambda_{u,2}^2, \lambda_{u,3}^2, \lambda_{u,4}^2\}$ for $\lambda_{u,1}^2 \geq \lambda_{u,2}^2 \geq \lambda_{u,3}^2 \geq \lambda_{u,4}^2$, and the corresponding eigenvectors, $\mathbf{U}_u = (\mathbf{u}_{u,1}\ \mathbf{u}_{u,2}\ \mathbf{u}_{u,3}\ \ \mathbf{u}_{u,4})$, are derived. The two highest eigenvalues and the corresponding eigenvectors for each MS are selected for the CSI feedback in the case of Rank-4 MU-MIMO, since two data streams are multiplexed per MS. Furthermore, the SINR for the i-th data stream (i = 1 or 2) of the u-th MS is calculated by $\gamma_{u,i} = \lambda_{u,i}^2 S_u/\sigma_u^2$, where σ_u^2 is the average noise power estimated using the received CSI-RS.

Figure 2(a) shows the bit fields per SB for the CSI feedback. Each complex eigenvector component is quantized by 13 b at maximum, which comprise N_P b for phase and N_A b for amplitude, using star-type mapping as shown in Figure 2(b) for each transmitter antenna and data stream. Thus, the quantized phase in radians and the amplitude component are represented in the following equations.

$$\text{(Quantized phase)} = 2\pi \times p/2^{N_P}, \quad (p = 0, 1, \ldots, 2^{N_P} - 1), \tag{1}$$

and

$$\text{(Quantized amplitude)} = \begin{cases} 1 & (N_A = 0) \\ q/2^{N_A} & (\text{otherwise}) \end{cases}, \quad (q = 0, 1, \ldots, 2^{N_A} - 1). \tag{2}$$

The eigenvalue and SINR for each data stream are quantized by 5 and 7 b, respectively. Therefore, the total number of CSI feedback bits per MS for Rank-4 MU-MIMO becomes $5 \times N_S \times \{8 \times (N_P + N_A) + 24\}$ b. In the article, we evaluate the influence of the number of quantization bits for the eigenvectors, that is, N_P and N_A, on the achievable throughput, since these parameters have a great impact on the total number of CSI feedback bits. The MS feeds back the quantized CSI to the BS via the uplink shared channel.

Precoding Weight Generation Scheme

At the BS transmitter, the precoding weights for downlink MU-MIMO are calculated based on the CSI transmitted from the two MSs. The precoding weight matrix for each SB is calculated based on the minimum mean square error criteria [6]. We note that the generated precoding weights are multiplied to both the data signal and DM-RS for each data stream.

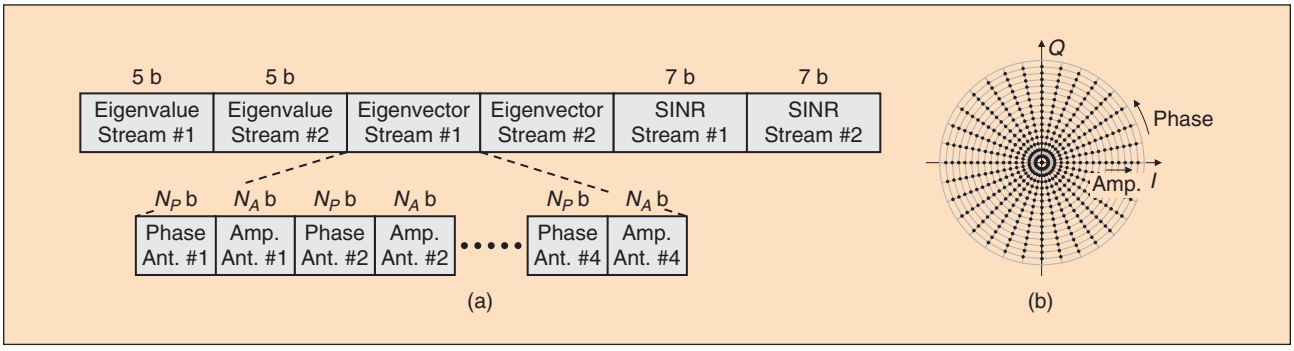


Figure 2 CSI feedback quantization. (a) Bit fields per SB for CSI feedback. (b) Quantization of eigenvector (e.g., N_P=5, N_A=4).

Configuration of Implemented LTE-Advanced Transceiver

Implemented OFDMA Transmitter and Receiver

The major radio link parameters and configuration of the implemented transceiver are given in Table 1 and Figure 3, respectively. The transmission bandwidth and the number of subcarriers of the OFDMA signal in the downlink are 90 MHz and 6000, respectively (thus, the subcarrier separation is 15 kHz). We employ CA using 5 CCs (each CC has an 18 MHz transmission bandwidth, which is supported in LTE Release 8) with contiguous spectrum allocation. In this article, F_{CSI} and T_{CSI} for MU-MIMO operation are set to 900 kHz (= 5 RBs) and 5 ms, respectively. In the BS transmitter, the information binary data sequence for each data stream and CC is independently turbo encoded and data modulated using QPSK, 16QAM, or 64QAM. After multiplying the precoding weights for MU-MIMO, the data sequence for each transmitter antenna is converted into an OFDMA symbol with the duration of 66.67 μs using an 8192-point inverse fast Fourier transform followed by the addition of a cyclic prefix (CP) of 4.69 μs. After conversion into baseband in-phase (I) and quadrature (Q) components using digital-to-analog (D/A) converters, quadrature modulation is performed. Finally, the intermediate frequency (IF) modulated signal is up-converted into the RF signal and amplified by the power amplifier, where the center carrier frequency is 3.92625 GHz.

TABLE 1 Major radio link parameters.

Carrier frequency		3.92625 GHz
OFDM signal bandwidth		90 MHz (18 MHz × 5 CCs)
Number of subcarriers		6000 (1200 × 5 CCs)
Subcarrier separation		15 kHz
Subframe length		1 ms (14 OFDM symbols)
OFDM symbol duration	Effective data	66.67 μs
	Cyclic prefix	4.69 μs
Number of antennas		BS: 4, MS: 2
Number of MSs		2
Channel coding/decoding		Turbo coding/ Max-Log-MAP decoding (6 iterations)
Channel model (laboratory experiment)		6-path exponentially-decayed Rayleigh fading model (parameters: f_D, σ_{path})
SB size (F_{CSI})		900 kHz (5 RBs)
CSI-RS transmission period (T_{CSI})		5 ms
Control delay for CSI feedback		10 ms
HARQ	Packet combining	Incremental redundancy
	Maximum number of transmissions	3
	Round trip delay	8 ms

At each MS receiver, we apply two-branch antenna diversity reception. The frequency down-converted IF signal is first linearly amplified by an automatic gain control amplifier with the dynamic range of approximately 50 dB. The received signal is converted into baseband I and Q components by a quadrature detector. The I and Q signals are converted into a digital format using 14-b analog-to-digital (A/D) converters.

After the CP is removed, the OFDMA signal is demultiplexed into each subcarrier component using an 8192-point FFT. Channel estimation for MIMO signal detection is performed for each SB using the DM-RS. The signal detection scheme based on the maximum likelihood detection (MLD) is applied to separate the two data streams that are transmitted to its own MS. Furthermore, an interference whitening filter is applied before the MLD operation in order to randomize the interfering data streams that are transmitted to the other MS [11], [12]. Finally, the sequence of likelihood values after MLD is turbo decoded using the Max-Log-MAP algorithm with six iterations to recover the transmitted binary data.

Table 2 summarizes the set of ten modulation and coding scheme sets used for AMC in the experiments. In order to compensate for the fluctuation in the reported SINR values, the threshold for MCS selection is adaptively adjusted by using outer-loop control based on acknowledgement (ACK)/negative ACK (NACK) feedback signaling from the MS [13]. The control delay of AMC is 10 ms. We use incremental redundancy for HARQ with packet combining and the round trip delay is 8 ms.

Configuration of Laboratory and Indoor Experiments

The configuration for the laboratory experimental system employing the multipath fading simulators is shown in Figure 4. The fading simulators generate a six-path exponentially decayed power delay profile with the root mean squared (r.m.s.) delay spread value of σ_{path}, where the relative path power is decayed by 2 dB and each path is independently Rayleigh-faded with the maximum Doppler frequency of f_D. Then, additive white Gaussian noise (AWGN) is added at the input of each receiver antenna for each MS. The average received signal-to-noise power ratio (SNR) for each MS

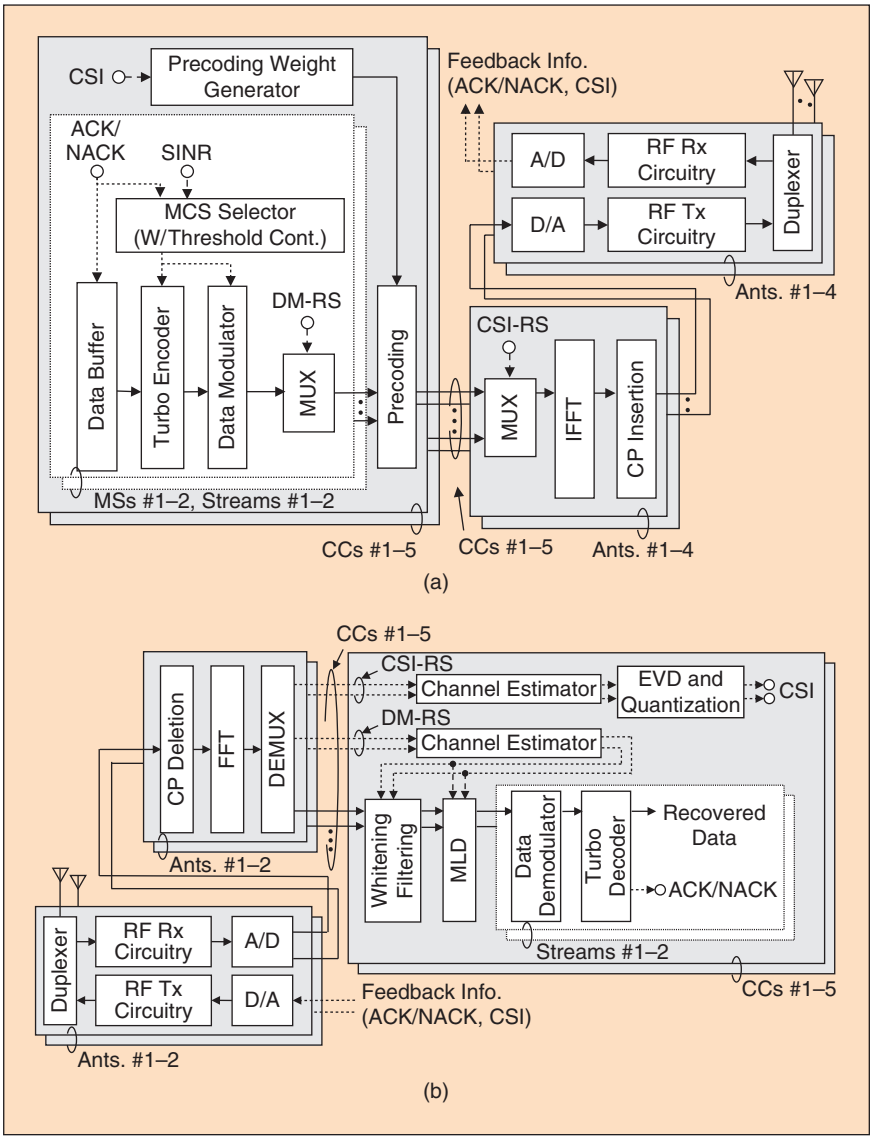


FIGURE 3 Configuration of implemented LTE-Advanced transceiver. (a) BS transmitter. (b) MS receiver.

is assumed to be the same in the experiments. We evaluate two antenna scenarios, including correlated and uncorrelated BS transmitter antennas. In the correlated antenna scenario, we assume two highly correlated transmitter antenna pairs. The fading correlation within the pair is set to 0.99 and that between antenna pairs is set to zero assuming a cellular environment for high-elevation BS antennas with a relatively narrow multipath angular spread. In the scenario, we set $\sigma_{path} = 0.03\ \mu s$ and $f_D = 10$ Hz corresponding to the moving speed of approximately 3 km/h at the carrier frequency of 3.92625 GHz. Furthermore, the direction of departure (DoD) for the u-th MS, DoD_u, is set to $\{\mathrm{DoD}_1/\mathrm{DoD}_2\} = \{+30/-30\}$ degrees. In the uncorrelated antenna scenario, the fading correlation among four transmitter antennas is set to zero. In this case, we set $\sigma_{path} = 0.03\ \mu s$ and $f_D = 1$ Hz assuming an indoor/small cell environment. In both scenarios, the fading correlation between the two receiver antennas of each MS is set to zero.

Throughput Performance Using AMC and HARQ

Here, we present the basic throughput performance when the number of quantization bits for CSI feedback is sufficiently large, that is, $N_P = 7$ and $N_A = 6$ b. Figure 5(a) and (b) shows the throughput performance using AMC and HARQ for MU-MIMO and SU-MIMO, which is defined as the aggregated throughput for each MS, as a function of the average received SNR per receiver antenna in the correlated and uncorrelated antenna scenarios, respectively. Figure 5(a) shows that, in the correlated antenna scenario, the peak throughput of 1 Gb/s and 570 Mb/s is achieved for MU-MIMO and SU-MIMO, respectively. Furthermore, assuming rank adaptation, that is, switching the number of data streams per MS according to the channel conditions, the required average received SNR to achieve the throughput of 500 Mb/s for MU-MIMO is significantly reduced by approximately 7 dB compared with that for SU-MIMO. In the uncorrelated antenna scenario, the peak throughput of 900 Mb/s is achieved for MU-MIMO

TABLE 2 MCS sets for AMC.

Index	*Modulation*	*Coding Rate*	*Index*	*Modulation*	*Coding Rate*
1	QPSK	0.39	6	64QAM	0.47
2		0.47	7		0.56
3	16QAM	0.38	8		0.65
4		0.49	9		0.73
5		0.58	10		0.78

as shown in Figure 5(b). The figure also shows that improvement in the required average received SNR to achieve the throughput of 500 Mb/s compared with that for SU-MIMO becomes small by approximately 2.5 dB.

WE EVALUATE TWO ANTENNA SCENARIOS, INCLUDING CORRELATED AND UNCORRELATED BS TRANSMITTER ANTENNAS.

Influence of Number of CSI Feedback Quantization Bits on Throughput

Next, we present the influence of the number of CSI feedback quantization bits on the achievable throughput for MU-MIMO and SU-MIMO. Figure 6 shows the throughput performance using AMC and HARQ for Rank-4 MU-MIMO when N_P and N_A are parameterized as 3–7 and 0–6 b, respectively, at the average received SNR of 26.2 dB. Each figure indicates the performance for the correlated and uncorrelated antenna scenarios, respectively. From these results, we find that the achievable throughput in the correlated antenna scenario is robust against N_P and N_A compared to that in the uncorrelated antenna scenario. This is because it is necessary to generate the precoding weights for MU-MIMO according to the antenna independent fading variation in the uncorrelated antenna scenario, and thus the influence of the quantization error is further emphasized. In both scenarios, we note that the throughput for $N_A = 1$ b is lower than that for $N_A = 0$ b. The reason for this is considered to be that the quantized amplitude becomes zero with high probability when $N_A = 1$ as can be understood from (2). Consequently, the required total number of quantization bits for the eigenvector, that is, $N_P + N_A$, to achieve the amount of degradation within 10% of the throughput for $N_P = 7$ and $N_A = 6$ b is 5 ($N_P = 5$ and $N_A = 0$) b and 8 ($N_P = 4$ and $N_A = 4$) b or more in the correlated and uncorrelated antenna scenarios, respectively. Table 3 summarizes the achievable throughput using AMC and HARQ for Rank-4 and Rank-2 MU-MIMO, and Rank-2 and Rank-1 SU-MIMO at the average received SNR of 26.2, 12.2, 16.2, and 8.2 dB, respectively, when $N_P + N_A$ is parameterized from 5 to 13 b. In the evaluations, the best combination of N_P and N_A is assumed regarding the total number of quantization bits. Table 3 illustrates that the amount of throughput degradation for Rank-2 MU-MIMO and SU-MIMO is within 10% in both antenna scenarios even when $N_P + N_A = 5$ b. Therefore, we find that the achievable throughput for Rank-2 MU-MIMO and SU-MIMO is robust against the CSI feedback quantization.

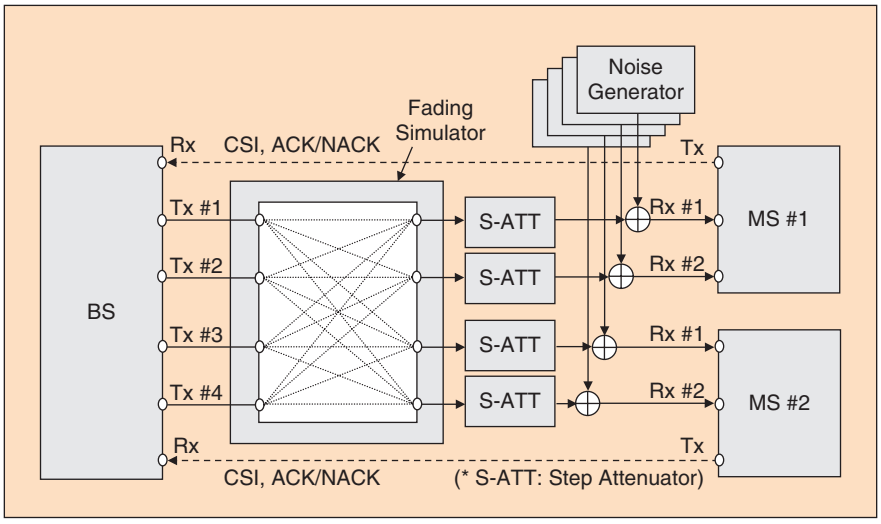


FIGURE 4 Configuration of laboratory experimental system.

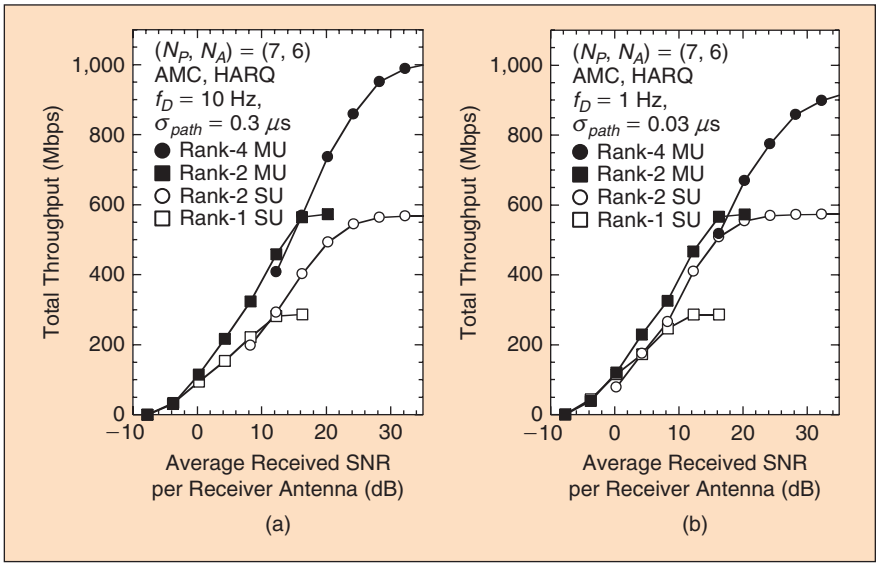


FIGURE 5 Throughput performance for MU-MIMO and SU-MIMO using AMC and HARQ. (a) Correlated antenna scenario. (b) Uncorrelated antenna scenario.

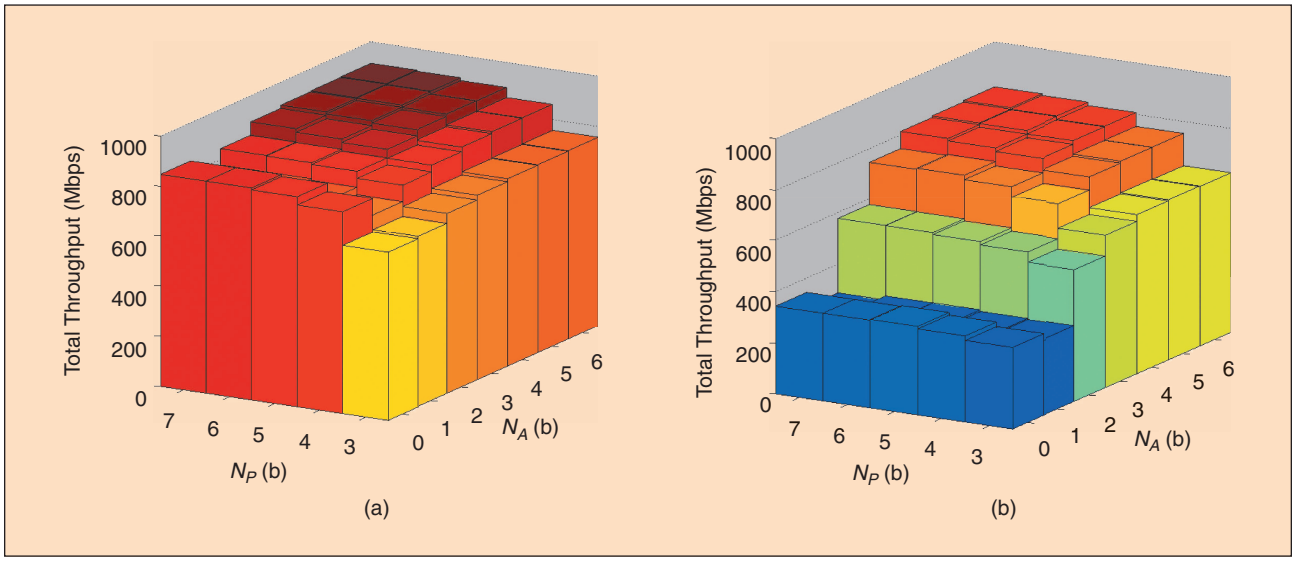


FIGURE 6 Influence of number of quantization bits on eigenvector (Rank-4 MU-MIMO). (a) Correlated antenna scenario. (b) Uncorrelated antenna scenario.

Figures 7(a) and (b) shows the throughput performance using AMC and HARQ for MU-MIMO as a function of the average received SNR per receiver antenna in the correlated and uncorrelated antenna scenarios, respectively, when $N_P + N_A$ is parameterized from 5 to 13 b. Figure 7(a) shows that, in the correlated antenna scenario, although when $N_P + N_A$ equaling 9 or more b is required to achieve the peak throughput of 1 Gb/s, the throughput performance for Rank-4 MU-MIMO is relatively robust against the CSI feedback quantization. For instance, the peak throughput of approximately 950 Mb/s is achieved even when $N_P + N_A = 5$ b. In the uncorrelated antenna scenario, we clearly find that $N_P + N_A$ of 9 or more b is required to obtain sufficient throughput gain of Rank-4 MU-MIMO as shown in Figure 7(b).

Indoor Experimental Results

We also investigate the influence of the number of CSI feedback quantization bits on the throughput performance for MU-MIMO in a conference room at the NTT DOCOMO R&D Center, which is representative of an indoor office environment. The dimensions, that is, width, depth, and height, of the room are 18.4 m × 12.2 m × 3.8 m, and 40 office desks with the height of 70 cm and 80 office chairs are arranged in the room. Figure 8 shows the BS-antenna arrangement, MS arrangement, and the measurement course. The BS antennas are located at the center of the room, and four antennas are linearly arranged with the adjacent antenna separation of 7.6 cm (corresponds to the wavelength of the carrier frequency, i.e., 1.0 λ). MS #1 is static and placed at one end of the room around Point A. MS #2 travels along the course with the entire length of approximately 14 m from Point A to Point B with the moving speed of approximately 1 km/h ($f_D = 3.6$ Hz). Two MS

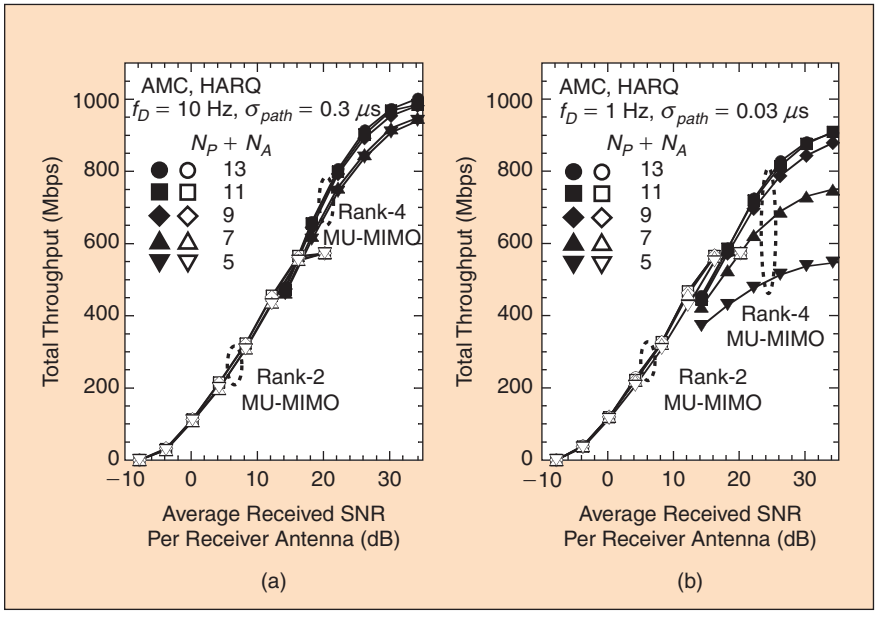


FIGURE 7 Throughput performance for MU-MIMO with quantized CSI feedback. (a) Correlated antenna scenario. (b) Uncorrelated antenna scenario.

antennas are arranged with the antenna separation of 7.6 cm (1.0 λ). The BS and MS antennas are dipole antennas with omni-directional beam patterns in azimuth with the gain of approximately 2 dBi and placed at the height of 2.4 m and 1.4 m from the floor, respectively. In the indoor experiments, the BS transmission power is set to 20 dBm (= 100 mW). Over the entire course, the BS antennas are in direct view from the MS antennas, that is, line-of-sight (LOS) conditions. The r.m.s. delay spread and the fading correlation between the adjacent BS transmitter antennas and the adjacent MS receiver antennas of the measurement course, which are calculated based on the received CSI-RSs, are approximately $\sigma_{path} = 0.05\ \mu s$, 0.42, and 0.30, respectively. Thus, the indoor environment in Figure 8 is broadly similar to the uncorrelated antenna scenario.

TABLE 3 Impact of $N_P + N_A$ on achievable throughput.

$N_P + N_A$	*Correlated Antenna Scenario*				*Uncorrelated Antenna Scenario*			
	MU-MIMO		*SU-MIMO*		*MU-MIMO*		*SU-MIMO*	
	Rank-4 (26.2 dB)	*Rank-2 (12.2 dB)*	*Rank-2 (16.2 dB)*	*Rank-1 (8.2 dB)*	*Rank-4 (26.2 dB)*	*Rank-2 (12.2 dB)*	*Rank-2 (16.2 dB)*	*Rank-1 (8.2 dB)*
13	913.0	455.0	398.2	219.2	824.1	469.2	503.7	247.2
11	908.1 (−0.5%)	455.0 (0.0%)	397.9 (−0.1%)	219.2 (0.0%)	816.1 (−1.0%)	464.0 (−1.1%)	503.6 (0.0%)	246.2 (−0.4%)
9	889.8 (−2.5%)	452.1 (−0.6%)	397.6 (−0.2%)	218.9 (−0.1%)	788.6 (−4.3%)	463.1 (−1.3%)	503.1 (−0.1%)	246.1 (−0.4%)
7	846.1 (−7.3%)	436.1 (−4.2%)	395.4 (−0.7%)	217.4 (−0.8%)	691.5 (−16.1%)	452.9 (−3.5%)	502.3 (−0.3%)	245.1 (−0.8%)
5	838.2 (−8.2%)	432.2 (−5.0%)	388.5 (−2.4%)	214.7 (−2.1%)	515.8 (−37.4%)	425.6 (−9.3%)	494.3 (−1.9%)	243.9 (−1.3%)

Figure 9 shows the cumulative distribution function (CDF) of the measured throughput using AMC and HARQ for Rank-4 MU-MIMO in an indoor office environment when $N_P + N_A$ is parameterized from 5 to 13 b. The measured throughput is averaged over the duration of 200 ms. Based on the results of Figure 9, we confirm that the results exhibit the same tendency of the results that in the uncorrelated antenna scenario as shown in Figure 7(b). As a result, we find that $N_P + N_A$ of 9 or more bits is required to obtain the peak throughput of approximately 1 Gb/s for Rank-4 MU-MIMO in an indoor office environment.

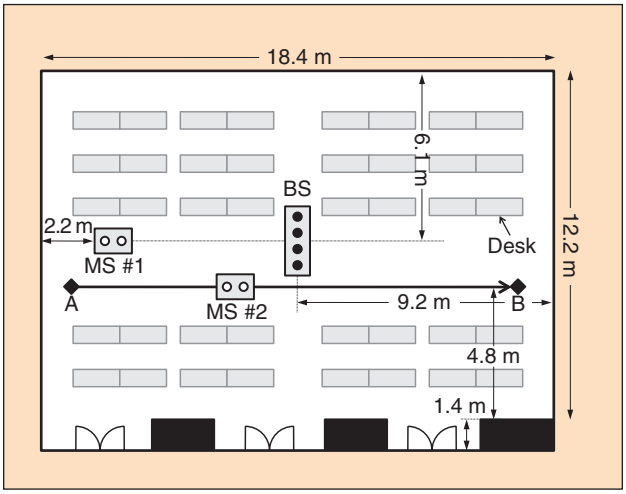


FIGURE 8 Environment for indoor experiment.

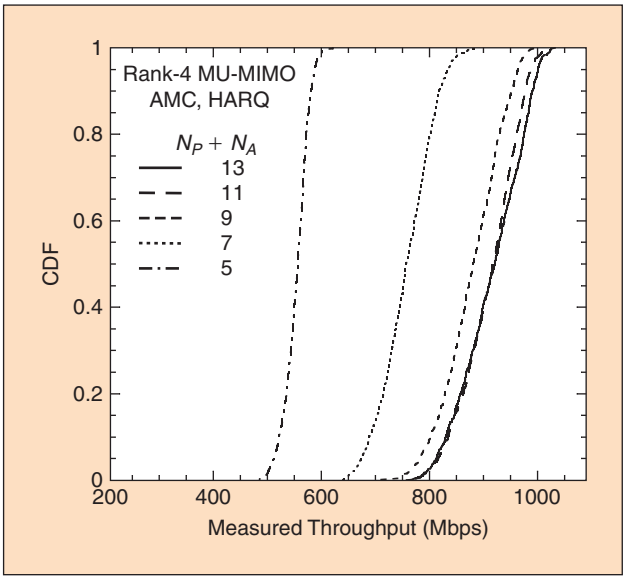


FIGURE 9 Indoor experimental results on the impact of $N_P + N_A$.

Conclusion

This article presented laboratory experimental results for four-by-two MU-MIMO applying extended CSI feedback based on EVD that achieves up to 1-Gb/s throughput using CA with 5 CCs in the LTE-Advanced downlink. The achievable throughput performance considering the influence of the number of CSI feedback quantization bits for the eigenvectors was evaluated using the implemented LTE-Advanced transceiver assuming two LTE-Advanced deployment scenarios, that is, cellular environments with correlated BS antennas and indoor/small cell environments with uncorrelated BS antennas. Laboratory experimental results showed that, in the correlated antenna scenario, the throughput performance for Rank-4 MU-MIMO is relatively robust

We find that the achievable throughput for Rank-2 MU-MIMO and SU-MIMO is robust against the CSI feedback quantization.

against the CSI feedback quantization although nine or more CSI feedback quantization bits per SB are required to achieve the peak throughput of 1 Gb/s. Meanwhile, in the uncorrelated antenna scenario, we clarified that nine or more quantization bits per SB are clearly required to obtain a sufficient throughput gain of Rank-4 MU-MIMO. The results also showed that the achievable throughput for Rank-2 MU-MIMO and SU-MIMO is robust against the CSI feedback quantization. Furthermore, we confirm that the same tendency occurred in an indoor office environment based on a real indoor propagation experiment.

Author Information

Yuichi Kakishima received the B.S. and M.S. degrees from Tokyo Institute of Technology, Tokyo, Japan, in 2005 and 2007, respectively. In 2007, he joined NTT DOCOMO, INC. Since joining NTT DOCOMO, he has been engaged in the research and development of wireless access technologies including multiple-antenna transmission techniques for LTE and LTE-Advanced systems. He was a recipient of the IEICE Young Engineer Award in 2011 and the 2011 Active Research Award in Radio Communication Systems from the IEICE.

Teruo Kawamura received the B.E. and M.E. degrees from Hokkaido University, Sapporo, Japan, in 1999 and 2001, respectively. In 2001, he joined NTT DOCOMO, INC. Since joining NTT DOCOMO, he has been engaged in the research and development of an uplink multiple access scheme for LTE and LTE-Advanced systems and wireless access technologies including equalization and interference cancellation for mobile communication systems. He is currently an assistant manager of the Radio Access Development Department of NTT DOCOMO.

Yoshihisa Kishiyama received the B.E., M.E., and Dr. Eng. degrees from Hokkaido University, Sapporo, Japan, in 1998, 2000, and 2010, respectively. In 2000, he joined NTT DOCOMO, INC. His research interests include advanced multiple access technologies with interference cancellation and future network concepts for efficient deployments and spectrum utilization. He was a recipient of the IEICE Young Engineer Award in 2004, and a recipient of the ITU Association of Japan Award in 2012. He is currently a manager of the Radio Access Development Department of NTT DOCOMO.

Hidekazu Taoka received the B.S. and M.S. degrees from the Department of Physics, Kyoto University, Japan, in 1998 and 2000, respectively, and the Dr. Eng. degree from Tohoku University, Sendai, Japan, in 2009. In 2000, he joined NTT DOCOMO, INC. Since joining NTT DOCOMO, he has been engaged in the research and development of wireless access technologies including multiple-antenna transmission techniques, relaying techniques, small cell and D2D interference management techniques, and future radio access techniques for mobile communication systems. Since June 2010, he has been working at DOCOMO Communications Laboratories Europe GmbH, Munich, Germany, as an expatriate from NTT DOCOMO. He is currently a manager of the infrastructure research group there.

Hidehiro Andoh received the B.S. and M.S. degrees from Kyusyu Institute of Technology, Fukuoka, Japan, in 1991 and 1993, respectively. In 1993, he joined NTT DOCOMO, INC. Since joining NTT DOCOMO, he has been engaged in the research and development of radio access technologies for W-CDMA mobile communications and broadband packet radio access technologies for LTE and LTE-Advanced. He is currently a manager of the Radio Access Development Department of NTT DOCOMO.

References

[1] 3GPP, TS 36.300 (V8.12.0), "Evolved Universal Terrestrial Radio Access (E-UTRA) and Evolved Universal Terrestrial Radio Access Network (E-UTRAN); Overall description," Apr. 2010.

[2] M. Tanno, Y. Kishiyama, N. Miki, K. Higuchi, and M. Sawahashi, "Evolved UTRA—physical layer overview," in *Proc. IEEE SPAWC*, June 2007, pp. 1–8.

[3] NTT DOCOMO. (2010, Nov. 8). [Online]. Available: http://www.nttdocomo.com/pr/2010/001494.html

[4] 3GPP, TS 36.201 (V10.0.0), "Evolved Universal Terrestrial Radio Access (E-UTRA); LTE physical layer; General description (Release 10)," Dec. 2010.

[5] E. Dahlman, S. Parkvall, and J. Sköld, *4G—LTE/LTE-Advanced for Mobile Broadband*. New York: Academic Press, 2011.

[6] Y. Kakishima, T. Kawamura, Y. Kishiyama, H. Taoka, and T. Nakamura, "Experimental evaluations on carrier aggregation and multi-user MIMO associated with EVD-based CSI feedback for LTE-Advanced downlink," in *Proc. IEEE ISWCS*, Nov. 2011, pp. 884–888.

[7] D. Love, R. Heath, V. Lau, D. Gesbert, B. Rao, and M. Andrews, "An overview of limited feedback in wireless communication systems," *IEEE J. Sel. Areas Commun.*, vol. 26, no. 8, pp. 1341–1365, Oct. 2008.

[8] M. Trivellato, F. Boccardi, and H. Huang, "On transceiver design and channel quantization for downlink multiuser MIMO systems with limited feedback," *IEEE J. Sel. Areas Commun.*, vol. 26, no. 8, pp. 1494–1504, Oct. 2008.

[9] C. Guthy, W. Utschick, and G. Dietl, "Finite rate feedback schemes for the MIMO OFDM broadcast channel," in *Proc. Int. ITG Workshop Smart Antennas WSA*, Feb. 2008, pp. 68–73.

[10] B. T. Smith, J. M. Boyle, and J. J. Dongarra, *Matrix Eigensystem Routines—EISPACK Guide* (Lecture Notes in Computer Science, no. 6), 2nd ed. New York: Springer-Verlag, 1988.

[11] D. Tse and P. Viswanath, *Fundamentals of Wireless Communication*, 2008.

[12] S. Shim, J. Kwak, R. H. Heath, and J. G. Andrews, "Block diagonalization for multi-user MIMO with other-cell interference," *IEEE Trans. Wireless Commun.*, vol. 7, no. 7, pp. 2671–2681, July 2008.

[13] J. Lee, R. Arnott, K. Hamabe, and N. Takano, "Adaptive modulation switching level control in high speed downlink packet access transmission," *3G Mobile Communication Technologies*, pp. 156–159, May 2002.

[14] 3GPP, "Feasible study for further advancements for E-UTRA (LTE-Advanced) (Release 10)," Tech. Rep. 36.912 (V10.0.0), Mar. 2011.

VT